

Density functional theory calculations and analysis for the reduction of NO by H₂ on Pd₆/TiO₂

Lixia Ling^{a,b}, Yueting Cao^a, Zhongbei Zhao^a, Ping Liu^b, Baojun Wang^{c,*}, Riguang Zhang^c, Debao Li^b

^a College of Chemistry and Chemical Engineering, Taiyuan University of Technology, Taiyuan 030024, Shanxi, People's Republic of China

^b State Key Laboratory of Coal Conversion, Institute of Coal Chemistry, Chinese Academy of Sciences, Taiyuan 030001, Shanxi, People's Republic of China

^c Key Laboratory of Coal Science and Technology (Taiyuan University of Technology), Ministry of Education and Shanxi Province, Taiyuan 030024, Shanxi, People's Republic of China

ARTICLE INFO

Keywords:

NO reduction
Density functional theory
Pd₆/TiO₂
Selectivity

ABSTRACT

Periodic density functional theory (DFT) calculations have been carried out to reveal the mechanism of NO reduction by H₂ on the Pd₆/TiO₂ catalyst. The favorable route for N₂ formation is NO → HNO → NHOH → N → N₂, and the rate-determining step is the formation of intermediate HNO via NO hydrogenation with an energy barrier of 103.0 kJ · mol⁻¹. The energy barriers of rate-determining steps for the formation of N₂O and NH₃ are 149.9 and 128.4 kJ · mol⁻¹, which are higher than that for N₂ formation, indicating that N₂ is the main product. Comparing with the reduction of NO on the Pd(2 1 1) surface, the reaction energy barrier for generating N₂ is obviously reduced, while the energy barrier for generating NH₃ has a little difference, which implies that Pd₆/TiO₂ shows better selectivity to N₂.

1. Introduction

Nitrogen oxides resulting from industrial and automotive exhausts have become severe challenge to environment over the past several decades, and many efforts have been made to reduce the NO_x emissions [1,2]. Currently, the selective catalytic reduction (SCR) of NO by hydrogen (SCR-H₂) has attracted more attention than SCR-NH₃ [3–5], since it is an environment-friendly technology and no secondary pollutants are produced [6]. In addition, H₂ is usually recognized as the efficient reducing agent at low temperature during the cold start engine. However, it is still under the development stage.

The catalysts of H₂-SCR are currently focused on the noble metal catalysts, which include theoretical and experimental studies, such as Pt [5], Au [7], Rh [8] and Pd [9]. Among them, Pd-based catalysts have advantages since they have good thermal stability and low-temperature activity. Zhang et al. [10] have investigated the reduction of NO on Pt-based and Pd-based catalysts, and Pd/Al₂O₃ has better activity than Pt/Al₂O₃ in the CO-H₂ reducing condition. The adsorption, dissociation and desorption of NO on Pd(1 1 1), (1 0 0) and (3 1 1) surfaces have been studied, and the results imply that NO is more easily to dissociation on the stepped Pd(3 1 1) surface [11]. NO reduction over stepped Pd(2 1 1) surface has also been investigated, the change of N₂ emission channel occurs at around 500 K, and the step edge is the activity site

[12]. Our recent study showed that Pd(2 1 1) surface exhibited higher catalytic activity to the reduction of NO with H₂ than that on the Pd(1 1 1) surface, and Pd(2 1 1) surface also showed higher selectivity for N₂ than NH₃ below about 500 K [13]. Additionally, NO adsorption and dissociation on subnanometer Pd_n clusters have been discussed, and the results suggest that the dissociation barrier of NO on the octahedral Pd cluster is lower than that on the icosahedral Pd cluster [14]. It can be seen that Pd is a good catalyst for NO reduction or activation. However, catalysts with different morphologies exhibit various properties.

Pd cluster catalysts are with high specific surface area [15] and high activity, which can also decrease the materials cost, and are widely used in hydrogenation [16], oxidation and reduction reaction [17,18]. TiO₂ has been widely used as catalyst carrier because of its good chemical and thermal stability [19], low cost and no toxicity. The supported Pd catalyst on the TiO₂ surface has been widely studied by experimental and theoretical in SCR reaction [20], which also showed good catalytic activity and selectivity for NO reduction [21,22]. Pd substituted TiO₂ catalyst (Ti_{0.99}Pd_{0.01}O_{2-δ}) has been synthesized and investigated for the catalytic reduction of NO by H₂, which showed the lowest N₂O formation and no NH₃ formation in the reaction [23]. Low-temperature NO_x reduction with H₂ + CO under oxygen-rich conditions over Pd/TiO₂/Al₂O₃ was studied, and a high NO_x conversion efficiency and good N₂ selectivity were obtained [24]. Further research showed that Pd/

* Corresponding author at: No. 79 West Yingze Street, Taiyuan University of Technology, Taiyuan 030024, People's Republic of China.
E-mail addresses: wangbaojun@tyut.edu.cn, wbj@tyut.edu.cn (B. Wang).

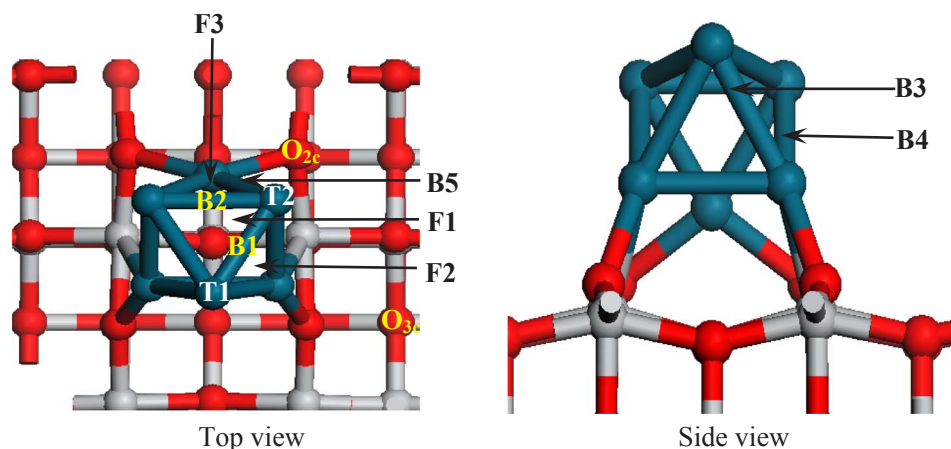


Fig. 1. The top and side views of Pd₆/TiO₂ model.

TiO₂ catalyst displayed very high NO_x conversions with good N₂ selectivity whereas Pd/Al₂O₃ delivered very low activity [25]. However, catalytic properties of catalysts vary with the size of clusters.

The stability for clusters is firstly needed to investigate. The stability of Pd clusters has been evaluated by the average binding energy, the second difference in energy and the energy gaps between the highest occupied molecular orbital (HOMO) and lowest unoccupied molecular orbital (LUMO) [26,27]. The average binding energy of Pd_n clusters showed that there was a little change and no longer increase with $n > 6$. Two order differential energies of Pd_n ($n = 4-6$) clusters were positive value, which indicated that Pd_n ($n = 4-6$) clusters were with good stability. Besides, Pd₆ cluster had the largest energy gap, which also implied Pd₆ cluster was relatively stable.

In this work, the model of Pd₆ cluster supported on the TiO₂ surface is firstly built. Subsequently, the adsorption and dissociation of NO, as well as correlated reactions are investigated. Further, the formation pathways of all possible products, including N₂, NH₃, N₂O and H₂O, are explored. Moreover, the activity and selectivity of Pd₆/TiO₂ catalyst will be obtained.

2. Computational details

2.1. Computational method

All calculations were performed in the Vienna ab initio simulation package (VASP) [28,29]. The exchange–correlation energies were described by the generalized gradient approximation (GGA) with the function of Perdew–Burke–Ernzerhof (PBE) [30] and the projector-augmented wave (PAW) [31,32] method was implemented to deal with electron–ion interactions. To expand the electron wave function, the cutoff energies for the plane-wave basis sets with 400, 500 and 600 eV were tested. The corresponding adsorption energies of NO on the Pd₆/TiO₂ at bridge site are -212.6 , -210.3 and $208.4 \text{ kJ} \cdot \text{mol}^{-1}$ with different cutoff energies, which indicates that cutoff energy of 400 eV is suitable and enough for our calculated systems. Additionally, it was widely used in previous work. [33–35]. A Gaussian smearing parameter of SIGMA = 0.2 eV was used to improve convergence of states near the Fermi level. The Brillouin zone sampling was carried out by using Monkhorst–Pack k -points of $2 \times 2 \times 1$ for supercell [36]. In addition, the van der Waals (vdW) interaction has also been investigated. Adsorption energies of NO on the Pd₆/TiO₂ at bridge site are -208.8 and $-212.6 \text{ kJ} \cdot \text{mol}^{-1}$ with and without vdW interaction. And there is very little difference of $2.5 \text{ kJ} \cdot \text{mol}^{-1}$ for the adsorption of HNO with and without vdW. They imply that the vdW interaction can be ignored, therefore, which is not considered in this work. Except for the fixed atoms, other atoms in the structure were fully relaxed until the electronic energy and force were smaller than 10^{-5} eV and $0.05 \text{ eV} \text{ \AA}^{-1}$,

respectively. To correct the underestimation of the intra-band Coulomb interactions, the GGA + U correction [37] was applied to treat the outer d electrons of the transition element Ti, and the value of U parameter was determined to be 4 eV for the Ti atom [38,39]. The activation barriers (E_a) are calculated as following equation:

$$E_a = E_{\text{TS}} - E_{\text{R}} \quad (1)$$

The adsorption energy E_{ads} , on the Pd₆/TiO₂ is defined by using the following equation:

$$E_{\text{ads}} = E_{\text{Pd}_6/\text{TiO}_2} + E_{\text{adsorbate}} - E_{\text{Pd}_6/\text{TiO}_2 - \text{adsorbate}} \quad (2)$$

where $E_{\text{Pd}_6/\text{TiO}_2 - \text{adsorbate}}$ is the total energy of the perfect Pd₆/TiO₂ and adsorbates system in its equilibrium state, $E_{\text{Pd}_6/\text{TiO}_2}$ is the energy of Pd₆/TiO₂, and $E_{\text{adsorbate}}$ is the energy of the isolated adsorbates.

The O-vacancy formation energy (E_{form}) is calculated as following equation:

$$E_{\text{form}} = E_{\text{Pd}_6/\text{TiO}_2}^{\text{O-vac}} + E^{\text{O}} - E_{\text{Pd}_6/\text{TiO}_2} \quad (3)$$

where $E_{\text{Pd}_6/\text{TiO}_2}^{\text{O-vac}}$ is the total energy of the oxygen-vacancy Pd₆/TiO₂, E^{O} is the energy of an O atom.

The nudged elastic band algorithm in combination with the climbing-image (CI-NEB) methods [40,41] were used to locate the transition states (TS) and map out the minimum energy pathways about H₂-SCR on the Pd₆/TiO₂ surface.

2.2. Surface models

There are four polymorphs of TiO₂ crystals in nature, such as anatase, rutile, brookite and TiO₂(B) [42,43], in which anatase TiO₂ has better catalytic activity and is commonly used to be as a carrier. Although the (101) facet is more dominantly present in all facets of anatase TiO₂, the (001) facet shows good catalytic activity in some reactions [36] and it has been widely studied by experimental and theoretical in SCR reaction [20,44].

The anatase TiO₂(001) model with size (3 × 2) and thickness of 4 layers is constructed and the most stable Pd₆ cluster is loaded on the TiO₂(001) surface. The Pd₆ cluster is loaded on TiO₂(001) surface with different initial models and the most stable configuration of Pd₆/TiO₂ was obtained, as shown in Fig. 1. The binding energy is $338.2 \text{ kJ} \cdot \text{mol}^{-1}$ between Pd₆ and TiO₂(001) surface. The bottom two layers were kept frozen, while the others are allowed to relax in the calculation process. The isolated molecules were optimized in a large cell of $10 \times 10 \times 10 \text{ \AA}$. There are ten possible adsorption sites on the Pd₆/TiO₂ catalyst, including five bridge sites (B1–B5), three threefold hollow sites (F1–F3) and two top sites (T1–T2), are considered in the adsorption process, as shown in Fig. 1. B represents the bridge site, F represents the threefold hollow site and T represents the top site.

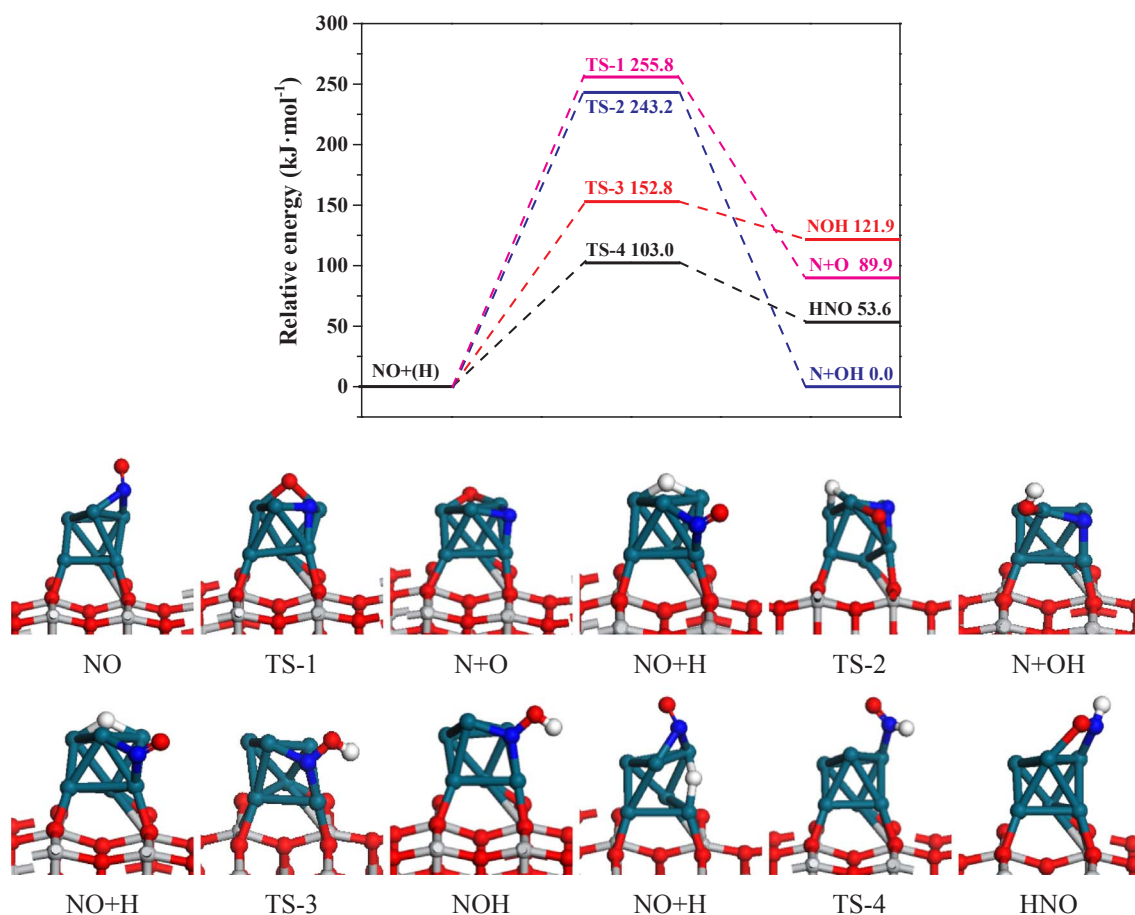


Fig. 2. Potential energy diagram of the NO dissociation and hydrogenation including corresponding configurations of initial states, transition states and final states.

3. Results and discussion

3.1. The related elementary reactions during the NO reduction

3.1.1. NO dissociation and hydrogenation

The activation of NO is the first step for the NO reduction, the adsorption and the direct dissociation of NO is firstly investigated. Two stable adsorption structures are obtained due to the similar adsorption energy. NO through the N atom connects to Pd atoms at B1 and F2 sites with adsorption energies of 212.6 and 218.8 $\text{kJ}\cdot\text{mol}^{-1}$, which is similar with the previous theoretical result of 217.1 $\text{kJ}\cdot\text{mol}^{-1}$ on pure Pd_8 cluster [14]. In situ DRIFTS study also showed that the adsorption of subsequent dissociation of NO occurred on metal sites in Pd/TiO₂ catalyst [25]. Dissociated N and O via NO were found to prefer adsorbing at F2 and B2 sites with adsorption energies of 445.5 and 414.9 $\text{kJ}\cdot\text{mol}^{-1}$, respectively. NO adsorbed at the B1 site directly dissociates into N and O via transition state TS-1 with a dissociation energy barrier of 255.8 $\text{kJ}\cdot\text{mol}^{-1}$ (Fig. 2), which is consistent with previous results of 242.2 and 248.0 $\text{kJ}\cdot\text{mol}^{-1}$ on pure cluster Pd_{13} and Pd_{25} [14]. It is clear that the direct dissociation reaction of NO is difficult due to the high energy barrier on the Pd_6/TiO_2 . The similar result is obtained on the Pd(1 1 1) surface, in which the direct dissociation of NO are not in favor [45]. Therefore, the reaction of hydrogen assisted dissociation and hydrogenation are further investigated.

Firstly, two stable adsorption configurations of H atom at F1 and F2 site with adsorption energies of 271.7 and 270.9 $\text{kJ}\cdot\text{mol}^{-1}$ are obtained. These results are in agreement with that on the Pd(2 1 1) surface with an adsorption energy of 269.2 $\text{kJ}\cdot\text{mol}^{-1}$ [46]. Secondly, hydrogen assisted dissociation of $\text{NO} + \text{H} \rightarrow \text{N} + \text{OH}$ has been considered. H captures O from NO resulting in N at F2 site and OH at T1 site via TS-2,

and the activation energy barrier is 243.2 $\text{kJ}\cdot\text{mol}^{-1}$. Although it is little lower than that of the direct dissociation, is still high with large energy barrier.

There are two possible reactions for the hydrogenation of NO leading to the formation of NOH and HNO. NO adsorbed at the F2 site reacts with H at the F1 site to NOH via transition state TS-3, and the activation energy barrier of the whole process is 152.8 $\text{kJ}\cdot\text{mol}^{-1}$. The formation of HNO via NO hydrogenation is also studied. NO at the B1 site and H at the F2 site combine to HNO via the transition state TS-4, and an energy barrier of 103.0 $\text{kJ}\cdot\text{mol}^{-1}$ is needed to be overcome.

It can be seen that the most favorable path of NO activation is NO hydrogenation to produce HNO from the above potential energy diagram, which has the lowest reaction activation energy barrier of 103.0 $\text{kJ}\cdot\text{mol}^{-1}$. It is consistent with that on the Pt(1 1 1) surface, in which the optimal path of NO activation is the hydrogenation of NO to generate HNO with the energy barrier of 97.4 $\text{kJ}\cdot\text{mol}^{-1}$ [47]. However, different results about the optimal path for NO activation are obtained on Pd(1 1 1) and Pd(2 1 1) surfaces. On the Pd(1 1 1) surface, H-assisted dissociation reaction is the most favorable path and the energy barrier is 152.4 $\text{kJ}\cdot\text{mol}^{-1}$ [45]. The favorable activation path of NO is $\text{NO} + \text{H} \rightarrow \text{NOH}$ with the energy barrier of 131.7 $\text{kJ}\cdot\text{mol}^{-1}$ on the Pd(2 1 1) surface [13]. It can also be seen that the optimal path about NO activation on the Pd_6/TiO_2 has lower activation energy barrier than that on Pd(1 1 1) and Pd(2 1 1) surfaces, implying that Pd_6/TiO_2 is more active than Pd(1 1 1) and Pd(2 1 1) surface for the activation of NO. In the following section, the correlated reactions of HNO will be carried out.

3.1.2. Correlated reactions of HNO

There are four possible elementary reactions of HNO, which are two

different hydrogenation reactions, the direct dissociation, and the hydrogenation dissociation. These possible elementary reactions are also considered in previous studies [8,45,47]. The hydrogenation reaction of HNO has two possible elementary reactions, as shown in Fig. 3. One is $\text{HNO} + \text{H} \rightarrow \text{NH}_2\text{O}$. The initial configuration is HNO adsorbed at the B1 site and H adsorbed at the F2 site, and the H atom attacks the N atom in HNO via the transition state TS-5 and finally the NH_2O is formed, which is adsorbed at the B1 site. The energy barrier of generating NH_2O via HNO hydrogenation is $91.5 \text{ kJ} \cdot \text{mol}^{-1}$. The other one is $\text{HNO} + \text{H} \rightarrow \text{NHOH}$, namely, HNO hydrogenation to form NHOH. HNO at the B1 site is attacked by the H atom, and the formed NHOH is adsorbed at the T2 position via the transition state TS-6 with an energy barrier of $71.8 \text{ kJ} \cdot \text{mol}^{-1}$. In addition to the possible hydrogenation reaction, the reactions about HNO also have dissociation reactions, including direct dissociation and hydrogen assisted dissociation. The direct dissociation reaction is HNO dissociation to form NH and O via TS-7, and an activation energy of $43.5 \text{ kJ} \cdot \text{mol}^{-1}$ is needed. For the hydrogen assisted dissociation reaction of HNO, the HNO at the B1 site reacts with H atom at the F1 position by the transition state TS-8 leading to NH and OH, and an energy barrier of $44.8 \text{ kJ} \cdot \text{mol}^{-1}$ is needed to be overcome.

It can be seen that the energy barrier of HNO hydrogenation to generate NH_2O is the highest in the related reactions of HNO, implying that it is difficult to occur comparing with other three steps. The energy barrier for the formation of NH from HNO via the direct dissociation and the hydrogen assisted dissociation is low, and the formation of NH is easy to happen. For the path of HNO hydrogenation generate NHOH, the barrier is $71.8 \text{ kJ} \cdot \text{mol}^{-1}$, which is higher than the energy barrier of NH generation, but lower than the formation of NH_2O species. In addition, previous work have shown that NHOH is an important intermediate during the reduction of NO by H_2 [13,47,48], which will lead to the formation of active N [47], so further studies on NHOH are carried out.

3.1.3. Correlated reactions of NHOH

Four related reactions of NHOH are investigated, and the potential energy diagram is shown in Fig. 4.¹ NHOH hydrogenation will lead to the formation of NH_2OH . In this step, the initial configuration is H atom adsorbed at the F1 site and the NHOH adsorbed at the T2 site. When the atom H attacks N atom of NHOH, NH_2OH is generated via transition state TS-9 with an energy barrier of $148.6 \text{ kJ} \cdot \text{mol}^{-1}$. NHOH hydrogenation will also lead to a dissociation to form NH and H_2O , in which H atom at the F2 site attacks the O atom of NHOH through transition state TS-10. The energy barrier is $73.9 \text{ kJ} \cdot \text{mol}^{-1}$. The direct dissociation of NHOH will lead to NH and OH via a cleavage of N–O bond, and the energy barrier is $61.8 \text{ kJ} \cdot \text{mol}^{-1}$. This process is similar to that on the Pt(1 1 1) surface with an energy barrier of $67.5 \text{ kJ} \cdot \text{mol}^{-1}$ at low coverage [47]. Another dissociation reaction is that N–O bond is cleaved followed by H transferring from N to O, and active N and H_2O are formed, which is a concerted step involving N–O and N–H bond cleavage and O–H bond formation. An energy barrier of $29.4 \text{ kJ} \cdot \text{mol}^{-1}$ is needed to overcome.

It can be seen that the reaction of generating N and H_2O is the most favorable path in the NHOH reactions according to the potential energy diagram, and the energy barrier is $29.4 \text{ kJ} \cdot \text{mol}^{-1}$. The same result is obtained on the Pt(1 1 1) surface, in which the dissociation of NHOH into N and H_2O is the most optimal pathway for NHOH related reactions at the low coverage [47]. The formation of NH_2OH is too difficult to happen due to a high energy barrier.

3.1.4. The favorable paths for forming active N and NH

As mentioned above, we can conclude that the most favorable path of generating active N is $\text{NO} \rightarrow \text{HNO} \rightarrow \text{NHOH} \rightarrow \text{N}$, and the most

favorable path for NH generation is $\text{NO} \rightarrow \text{HNO} \rightarrow \text{NH}$. Both rate-determining steps for forming active N and NH are the hydrogenation of NO to HNO with an activation energy of $103.0 \text{ kJ} \cdot \text{mol}^{-1}$. It is different from that on Pd(1 1 1) and Rh(2 2 1) surfaces. The H atom abstracting the O atom to form active N is the most favorable route on the Pd(1 1 1) surface, namely, $\text{NO} + \text{H} \rightarrow \text{N} + \text{OH}$. The energy barrier is $152.4 \text{ kJ} \cdot \text{mol}^{-1}$ [45]. The direct dissociation of NO to active N and O ($\text{NO} \rightarrow \text{N} + \text{O}$) is the feasible path on the Rh(2 2 1) surface with an activation energy of $120.6 \text{ kJ} \cdot \text{mol}^{-1}$ [8]. It can also be seen that the active N is easier to form over Pd_6/TiO_2 catalyst than that on Pd(1 1 1) and Rh(2 2 1) surfaces. The active species N and NH will generate the final products N_2 and NH_3 according to subsequent reactions. In addition, products N_2O and H_2O will also be investigated in the following sections.

3.2. Products generation

3.2.1. The generation of N_2

Active N is the important and major precursor for N_2 , which is formed via the hydrogenation of NO to HNO, the second hydrogenation to NHOH, and the dissociation of NHOH. Two active N can be directly connected to each other to generate N_2 . Two N atoms at F1 and F2 sites generate N_2 by TS-13 and the generated N_2 is adsorbed at the B1 site. The energy barrier of this process is only $52.8 \text{ kJ} \cdot \text{mol}^{-1}$. However, energy barriers of the combination of two adsorbed active N to N_2 were 177.5 and $142.5 \text{ kJ} \cdot \text{mol}^{-1}$ on Pd(1 1 1) [45] and Pd(2 1 1) [13] surfaces, respectively. And $\text{N} + \text{N} \rightarrow \text{N}_2$ was not the most favorable path to generate N_2 on these two surfaces. Compared with energy barriers of $\text{N} + \text{N} \rightarrow \text{N}_2$ on the above three catalysts, it is clearly that Pd_6/TiO_2 is easier to produce N_2 from active N than that on Pd(1 1 1) and Pd(2 1 1) surfaces [45,13].

The potential energy diagram for forming N_2 from NO in the condition of H_2 is shown in Fig. 5. It is also the most favorable path to generate N_2 , namely, $\text{NO} \rightarrow \text{HNO} \rightarrow \text{NHOH} \rightarrow \text{N} \rightarrow \text{N}_2$. The first step for the activation of NO via the hydrogenation is the rate-determining step in the whole reaction path of NO reduction to generate N_2 , which is represented by the red color in Fig. 5. The energy barrier of the rate-determining step is $103.0 \text{ kJ} \cdot \text{mol}^{-1}$. Certainly, the dimer path for the formation of N_2 during the NO reduction on the Pd_6/TiO_2 has also been considered. Unfortunately, the stable structure of dimer N_2O_2 is not obtained. Therefore, the dimer path is not shown in this work. Compared with Pd(2 1 1) and Pd(1 1 1) surfaces, the favorable reaction path, the rate-determining step and corresponding energy barrier of generating N_2 have changed. The main path of producing N_2 is the dimer path and the rate-determining step is $\text{N}_2\text{O}_2 \rightarrow \text{N}_2\text{O} + \text{O}$, and the corresponding energy barrier is $116.2 \text{ kJ} \cdot \text{mol}^{-1}$ on the Pd(2 1 1) surface [13]. But on the Pd(1 1 1) surface, the main path to generate N_2 is the NO hydrogenation dissociation into the active N, which finally generate N_2 . The rate-determining step is $\text{NO} + \text{H} \rightarrow \text{N} + \text{OH}$ and the reaction barrier is $152.4 \text{ kJ} \cdot \text{mol}^{-1}$ [45]. These results show that Pd_6/TiO_2 not only changes the main reaction path of H_2 reduction of NO, but also reduces reaction barrier of the rate-determining step, which indicates Pd_6/TiO_2 has better catalytic activity for the reduction of NO to produce N_2 than Pd(2 1 1) and Pd(1 1 1) surfaces.

3.2.2. The formation of N_2O

In addition to the direct production of N_2 via active N, the adsorbed N can also react with the adsorbed NO leading to the formation of N_2O . It can be seen from the configuration diagram in Fig. 6 that NO adsorbed at the B1 site reacts with the active N adsorbed at the F2 site via TS-14 leading to the formation of N_2O , and an energy barrier of $149.9 \text{ kJ} \cdot \text{mol}^{-1}$ is needed. The favorable path to form N_2O can be generalized in Fig. 6, we can see that the path to generate N_2O is $\text{NO} \rightarrow \text{HNO} \rightarrow \text{NHOH} \rightarrow \text{N} \rightarrow \text{N}_2\text{O}$. These steps to form active N are the same as that to generate N_2 . However, the rate-determining step of the whole reaction path is changed. $\text{NO} + \text{H} \rightarrow \text{HNO}$ is the rate-determining step

¹ For interpretation of color in Figs. 5 and 7, the reader is referred to the web version of this article.

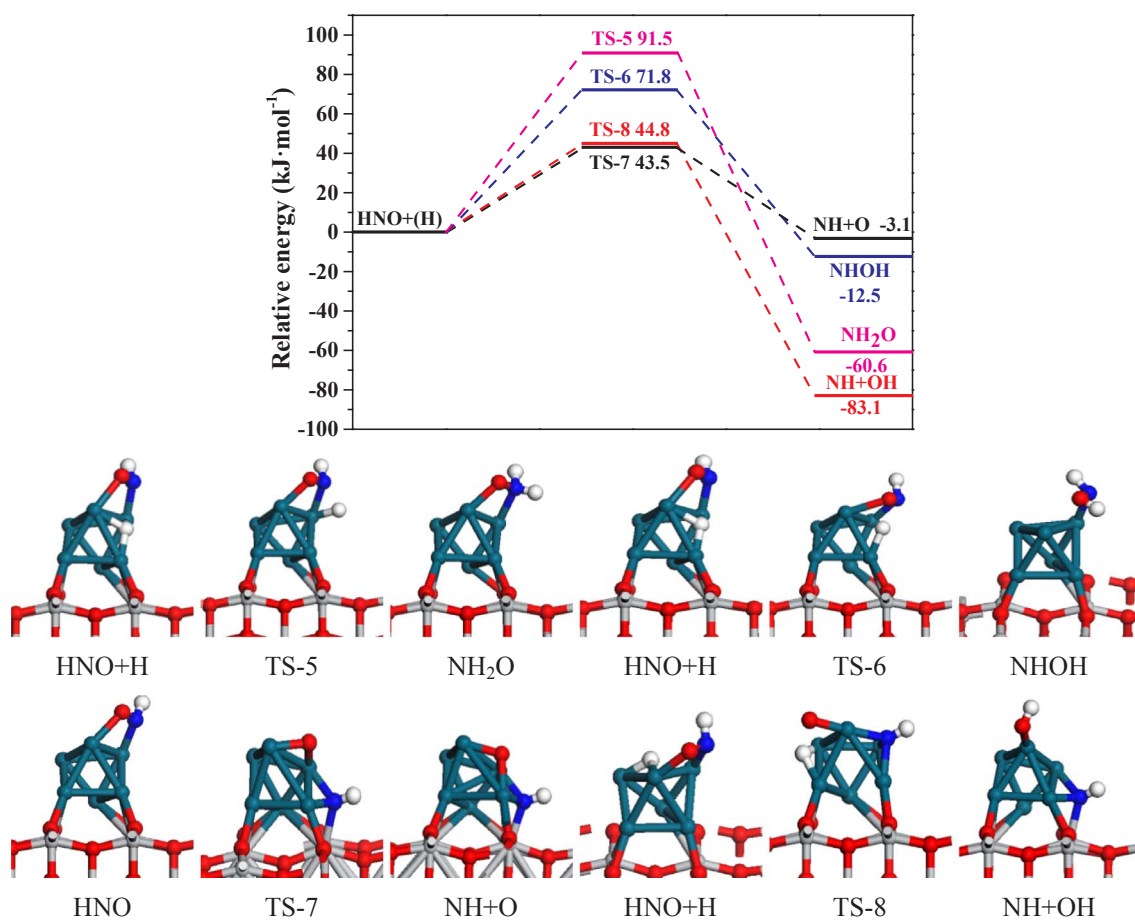


Fig. 3. Potential energy diagram of the HNO dissociation and hydrogenation including corresponding configurations of initial states, transition states and final states.

in the reaction path of generating N_2 , but in the process of generating N_2O , the rate-determining step is changed into $N + NO \rightarrow N_2O$. Energy barriers of rate-determining step to generate N_2 and N_2O are 103.0 and 149.9 $\text{kJ} \cdot \text{mol}^{-1}$, which shows that N_2O is a possible byproduct but is not easy to be generated since the energy barrier of producing N_2O is higher than that of producing N_2 on the Pd_6/TiO_2 . NO reduction by H_2 on $\text{Ti}_{0.99}\text{Pd}_{0.01}\text{O}_{2-8}$ was carried out in a temperature programmed reaction system equipped with a quadrupole mass spectrometer and a gas chromatograph, which shows the concentration of N_2O is the lowest in all products [23]. The decomposition of N_2O to N_2 is also calculated, but the transition state cannot be obtained, which implies that the N_2O dissociation is infeasible and N_2O is one of products during the NO reduction process over Pd_6/TiO_2 . The similar results are obtained on the $\text{Pd}(1\ 1\ 1)$, $\text{Pt}(1\ 1\ 1)$, $\text{Rh}(2\ 2\ 1)$ and $\text{Ni}(1\ 1\ 1)$ surface [45,49,8,50]. However, it is proved that N_2O is a key intermediate for N_2 generation on the $\text{Pd}(2\ 1\ 1)$ surface through theoretical calculation [13] and experimental study [12].

3.2.3. The generation of NH_3

NH_3 is a possible product during the reaction of NO by H_2 . The favorable NH species formation is the direct dissociation of HNO, which is different that on $\text{Rh}(2\ 2\ 1)$ [8], $\text{Pd}(1\ 1\ 1)$ [45] and $\text{Pd}(2\ 1\ 1)$ [13] surfaces, the hydrogenation of N is the main step for NH. NH eventually generates NH_3 via two gradual hydrogenation reactions. It can be seen from Fig. 7 that the most favorable path from NO to NH_3 is $\text{NO} \rightarrow \text{HNO} \rightarrow \text{NH} \rightarrow \text{NH}_2 \rightarrow \text{NH}_3$. In the potential energy diagram, the elementary reaction $\text{NH}_2 + \text{H} \rightarrow \text{NH}_3$ is expressed by red color, which is the rate-determining step of the whole NH_3 formation path, and the energy barrier is 128.4 $\text{kJ} \cdot \text{mol}^{-1}$. The formation energy barrier of NH_3 on the Pd_6/TiO_2 is slightly higher than that on $\text{Rh}(2\ 2\ 1)$ [8] and Pd

(1 1 1) [45] surfaces, in which the formation energy barrier of NH_3 are 112.9 ($\text{NH}_2 + \text{H} \rightarrow \text{NH}_3$) and 115.8 $\text{kJ} \cdot \text{mol}^{-1}$ ($\text{N} + \text{H} \rightarrow \text{NH}$), respectively. Compared with the energy barrier of 103.0 $\text{kJ} \cdot \text{mol}^{-1}$ for N_2 generation, the energy barrier of NH_3 formation is higher, which shows that NH_3 is not easy to generate on the Pd_6/TiO_2 .

3.2.4. The generation of H_2O

H_2O generation path is also studied in the process of NO reduction by H_2 . The maximum energy barrier of H_2O formation is 86.7 $\text{kJ} \cdot \text{mol}^{-1}$ on the Pd_6/TiO_2 (Fig. 8), while maximum energy barriers for producing H_2O on $\text{Pd}(1\ 1\ 1)$ [45] and $\text{Pd}(2\ 1\ 1)$ [13] surfaces are 121.6 and 123.0 $\text{kJ} \cdot \text{mol}^{-1}$, respectively. It implies that the formation energy barrier of H_2O on the Pd_6/TiO_2 is significantly reduced. The formed H_2O weakly adsorbs on the surfaces with an adsorption energy of 47.2 $\text{kJ} \cdot \text{mol}^{-1}$, which indicates that O and OH species are more easily released from Pd_6/TiO_2 catalyst via forming H_2O .

3.3. General discussion

Adsorption and reaction of all species occur on metal Pd except the adsorption of NH, which shows metal Pd are active sites. In addition, the formation energies of O-vacancy by removing surface $\text{O}_{2\text{C}}$ and $\text{O}_{3\text{C}}$ on the Pd_6/TiO_2 are 646.3 and 708.7 $\text{kJ} \cdot \text{mol}^{-1}$, which imply that surface O are very stable and cannot participate in the NO reduction reaction. The same result has been obtained that adsorption and subsequent dissociation of NO on reduced (Pd^0) metal sites on Pd/TiO_2 by an in situ DRIFTS [25].

The formation of active N goes through the favorable route is $\text{NO} + \text{H} \rightarrow \text{HNO} + \text{H} \rightarrow \text{NHOH} \rightarrow \text{N}$ on the Pd_6/TiO_2 , however, the optimal path for the formation of active N on the $\text{Pd}(1\ 1\ 1)$ surface is

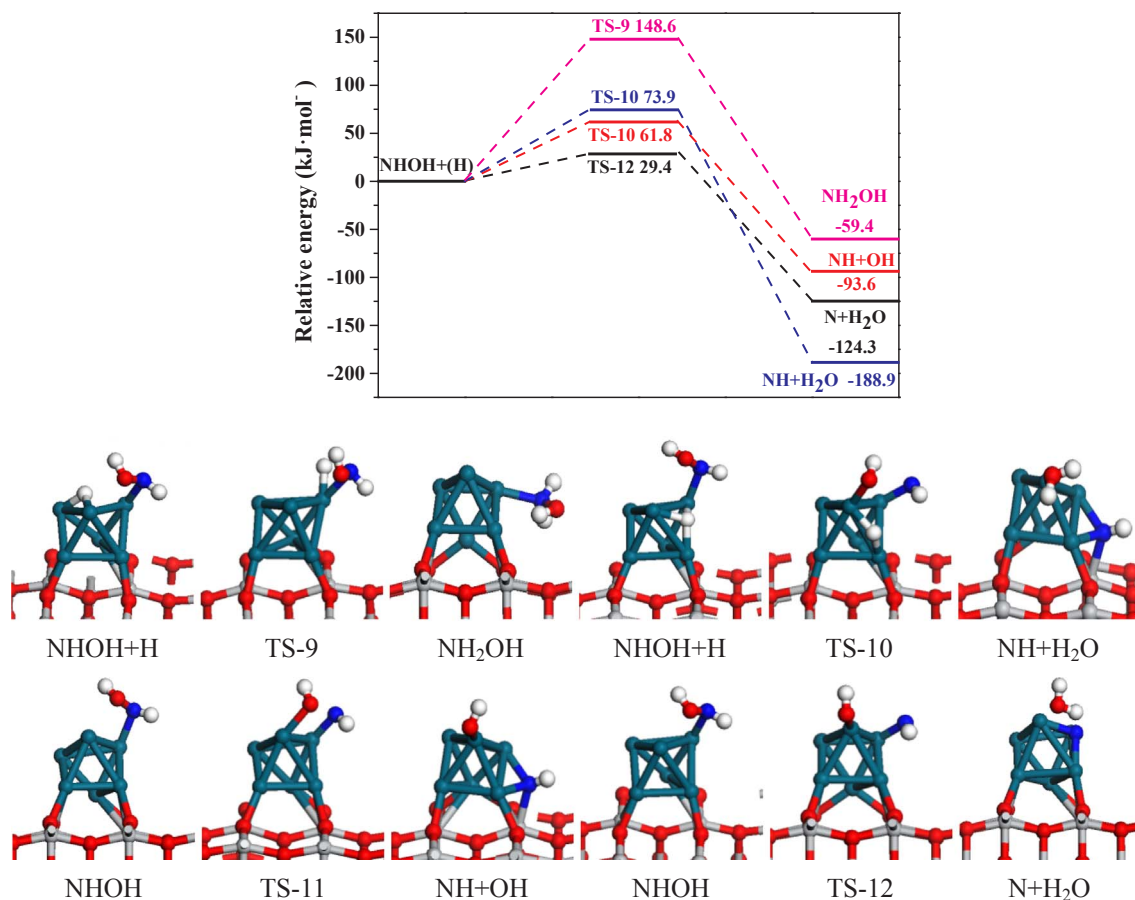


Fig. 4. Potential energy diagram of the NHOH dissociation and hydrogenation including corresponding configurations of initial states, transition states and final states.

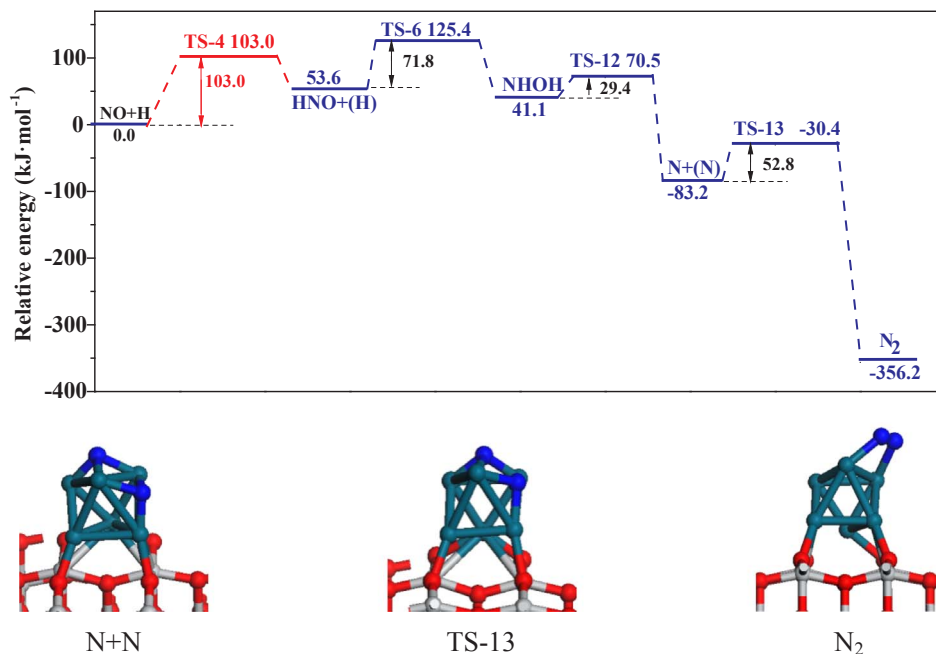


Fig. 5. Potential energy diagram of N₂ formation including corresponding configurations of initial states, transition states and final states.

$\text{NO} + \text{H} \rightarrow \text{N} + \text{OH}$ [45]. It can be seen that the optimal paths of N–O bond cleavage leading to active N are different on two catalysts. In addition, the rate-determining step and the corresponding energy barriers are also different. On the Pd₆/TiO₂, the rate-determining step is $\text{NO} + \text{H} \rightarrow \text{HNO}$ and energy barrier is $103.0 \text{ kJ}\cdot\text{mol}^{-1}$, while the rate-

determining step is $\text{NO} + \text{H} \rightarrow \text{N} + \text{OH}$ and the barrier is $152.4 \text{ kJ}\cdot\text{mol}^{-1}$ on the Pd(1 1 1) surface [45]. It implies that active N can be formed more easily on the Pd₆/TiO₂ than that on the Pd(1 1 1) surface.

There are three kinds of N-containing products, N₂, N₂O and NH₃ in

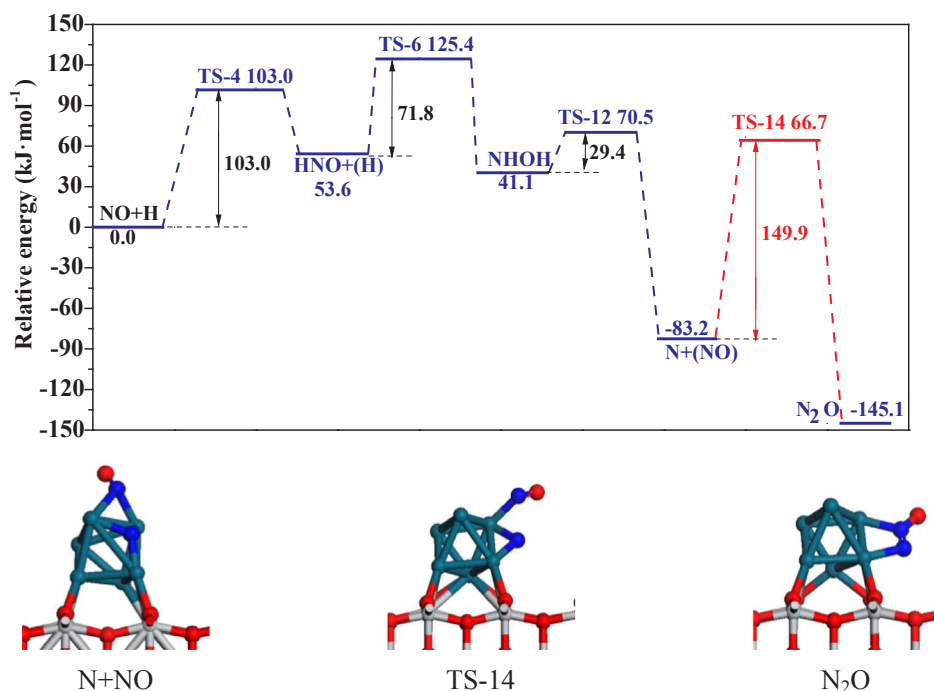


Fig. 6. Potential energy diagram of N_2O formation including corresponding configurations of initial states, transition states and final states.

the reduction of NO by H_2 on the Pd_6/TiO_2 . The rate-determining step of the N_2 generation process is $NO + H \rightarrow HNO$, which energy barrier is $103.0 \text{ kJ} \cdot \text{mol}^{-1}$. However, the highest activation energies occur at the dissociation of NO bond for the formation of N_2 are 152.4 and $116.2 \text{ kJ} \cdot \text{mol}^{-1}$ on $Pd(111)$ [45] and $Pd(211)$ [13] surfaces, respectively. Compared with the $Pd(111)$ and $Pd(211)$ surface, the barrier of rate-determining step has declined for the N_2 emission on the Pd_6/TiO_2 , which implies that Pd_6/TiO_2 exhibits higher catalytic activity to the reduction of NO by H_2 than that on the $Pd(111)$ and $Pd(211)$ surface. The rate-determining steps for producing N_2O and NH_3 are $N + NO \rightarrow N_2O$ and $NH_2 + H \rightarrow NH_3$, and the energy barriers are 149.9

and $128.4 \text{ kJ} \cdot \text{mol}^{-1}$ respectively. It can be seen from the energy barriers that the formation of N_2 is more favorable and the generation of by-product N_2O and NH_3 are difficult because of the high barrier on the Pd_6/TiO_2 .

In addition, the energy barrier of rate-determining for forming NH_3 and N_2 are 128.4 and $103.0 \text{ kJ} \cdot \text{mol}^{-1}$ on the Pd_6/TiO_2 and the difference value is $25.4 \text{ kJ} \cdot \text{mol}^{-1}$. Compared to the $Pd(211)$ surface [13], the energy barrier for forming NH_3 has a little difference (128.4 vs $131.7 \text{ kJ} \cdot \text{mol}^{-1}$), but a reduction of $13.2 \text{ kJ} \cdot \text{mol}^{-1}$ for generating N_2 . As a result, the productivity and selectivity of N_2 can be well improved on the Pd_6/TiO_2 . Moreover, no NH_3 formation was detected on

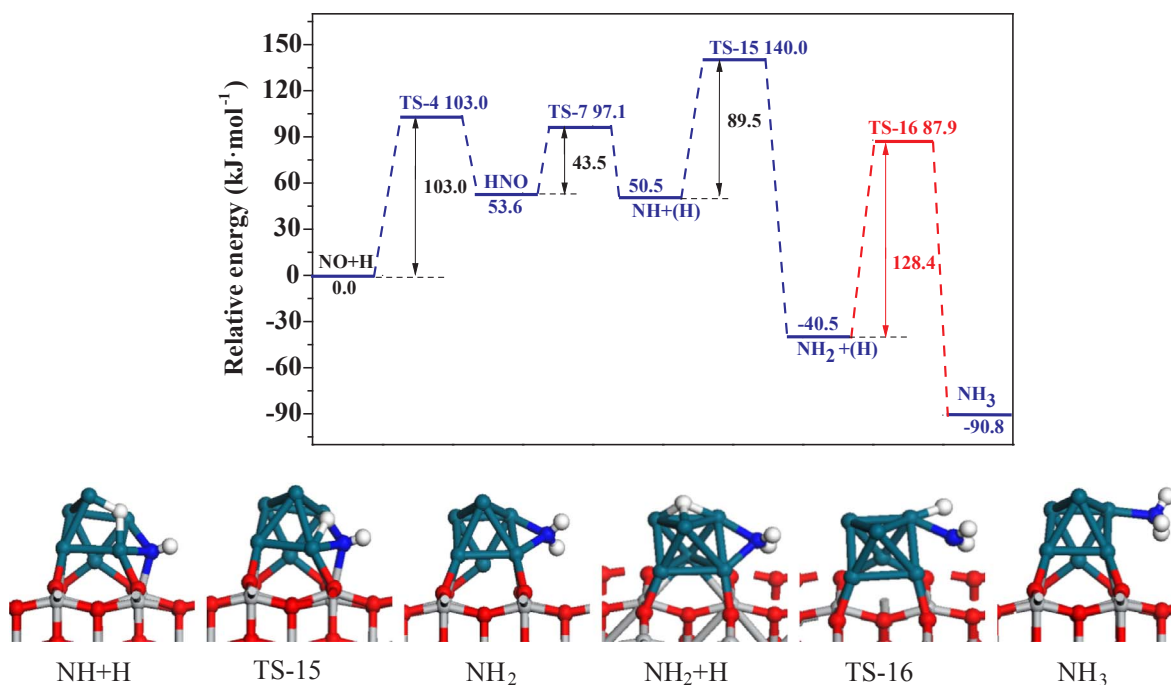


Fig. 7. Potential energy diagram of NH_3 formation including corresponding configurations of initial states, transition states and final states.

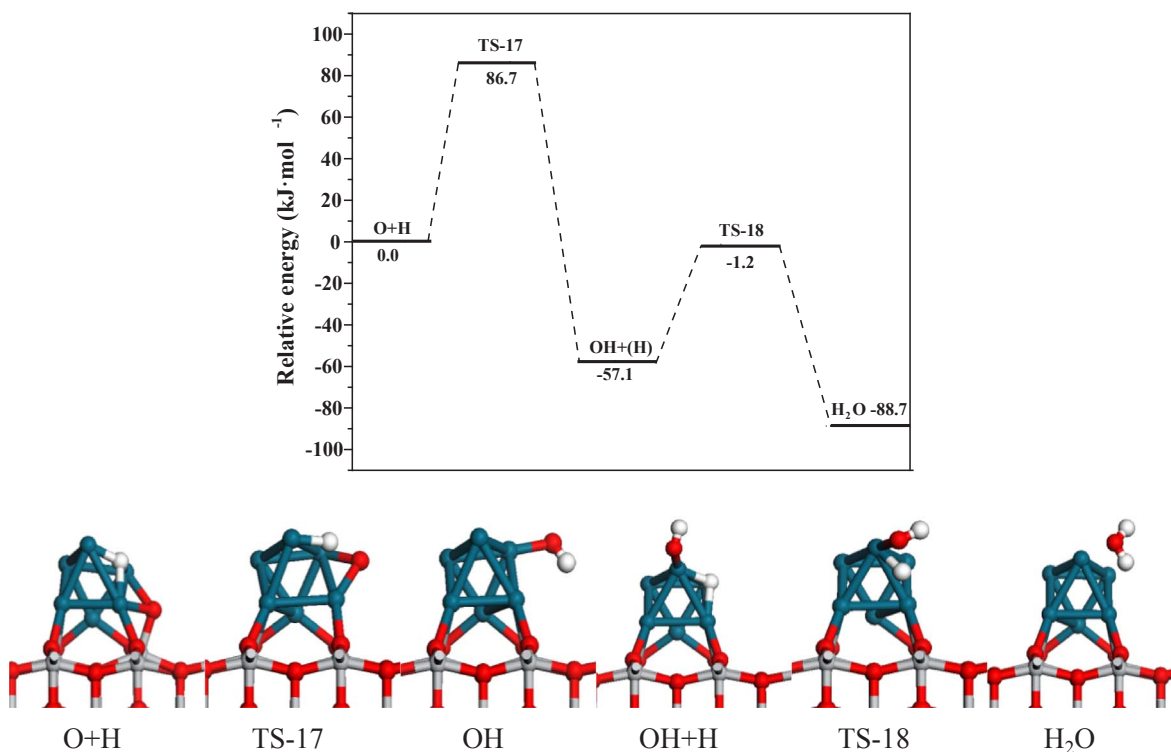


Fig. 8. Potential energy diagram of H₂O formation including corresponding configurations of initial states, transition states and final states.

Ti_{0.99}Pd_{0.01}O₂₋₈ during the NO reduction by H₂ by a quadrupole mass spectrometer and a gas chromatograph [23]. And the high N₂ selectivity was attributed to the reaction of formed NH_x intermediates with NO_x leading to N₂ [25]. During the reaction of NO reduction by H₂, NH is formed by the direct dissociation of HNO with a little energy barrier of 43.5 kJ·mol⁻¹, and the hydrogenation of NH to NH₂ needs a relative high energy barrier of 89.5 kJ·mol⁻¹. It shows that NH is the main species of NH_x. Therefore, the co-adsorption structure of NH and NO is first optimized in order to study the reaction of NH_x intermediates with NO_x. However, the stable co-adsorption structure is not obtained on the Pd₆/TiO₂.

4. Conclusions

In this work, the reduction of NO by H₂ on the Pd₆/TiO₂ has been studied by using the periodic density functional theory method. NO tends to hydrogenate leading to the formation of HNO, rather than the direct dissociation. And then, NHOH is generated through the hydrogenation of HNO. N is formed followed by the N–O bond cleavage of NHOH on the Pd₆/TiO₂. The reaction energy barrier shows that the Pd₆/TiO₂ can provide more active N than the Pd(1 1 1) surface.

In addition, the generation paths of N₂, N₂O and NH₃ are also studied and the result shows that N₂ and N₂O are produced via the active N, and the NH₃ is generated via two gradual hydrogenation reactions of NH formed by the direct dissociation of HNO. It can be seen from energy barrier of the rate-determining step that the formation of N₂ is more favorable and the generation of by-product N₂O and NH₃ is difficult because of the high barrier on the Pd₆/TiO₂. It also indicates Pd₆/TiO₂ shows a high selectivity to N₂.

Acknowledgements

We gratefully acknowledge financial support from the National Natural Science Foundation of China (Grant Nos. 21576178 and 21476155), the Key Projects of National Natural Science Foundation of China (21736007), Research Project Supported by Shanxi Scholarship

Council of China (No. 2016-030) and the Foundation of State Key Laboratory of Coal Conversion (No. J18-19-602).

References

- [1] Y. Hu, K. Griffiths, P.R. Norton, Surface science studies of selective catalytic reduction of NO: progress in the last ten years, *Surf. Sci.* 603 (2009) 1740–1750.
- [2] L. Chen, J. Li, M. Ge, The poisoning effect of alkali metals doping over nano V₂O₅-WO₃/TiO₂ catalysts on selective catalytic reduction of NO_x by NH₃, *Chem. Eng. J.* 170 (2011) 531–537.
- [3] C. Xu, W. Sun, L. Cao, J. Yang, Highly efficient Pd-doped ferrite spinel catalysts for the selective catalytic reduction of NO with H₂ at low temperature, *Chem. Eng. J.* 289 (2015) 231–238.
- [4] L. Wang, C. Yin, R.T. Yang, Selective catalytic reduction of nitric oxide with hydrogen on supported Pd: enhancement by hydrogen spillover, *Appl. Catal. A-Gen.* 514 (2016) 35–42.
- [5] G.G. Olympiou, A.M. Efstathiou, Industrial NO_x control via H₂-SCR on a novel supported-Pt nanocatalyst, *Chem. Eng. J.* 170 (2011) 424–432.
- [6] K. Okumura, T. Motohiro, Y. Sakamoto, H. Shinjoh, Effect of combination of noble metals and metal oxide supports on catalytic reduction of NO by H₂, *Surf. Sci.* 603 (2009) 2544–2550.
- [7] Y. Wang, D. Zhang, Z. Yu, C. Liu, Mechanism of N₂O formation during NO reduction on the Au(111) surface, *J. Phys. Chem. C* 114 (2010) 2711–2716.
- [8] L. Huai, T. Su, H. Wen, X. Jin, J. Liu, NO reduction by H₂ on the Rh(111) and Rh(221) surfaces: a mechanistic and kinetic study, *J. Phys. Chem. C* 120 (2016) 5410–5419.
- [9] G. Qi, R.T. Yang, F.C. Rinaldi, Selective catalytic reduction of nitric oxide with hydrogen over Pd-based catalysts, *J. Catal.* 237 (2006) 381–392.
- [10] Q. Zhang, L. Lv, J. Zhu, X. Wang, J. Wang, M. Shen, The effect of CO on NO reduction over Pt/Pd-based NSR catalysts at low temperature, *Catal. Sci. Technol.* 3 (2013) 1069–1077.
- [11] I. Nakamura, T. Fujitani, H. Hamada, Adsorption and decomposition of NO on Pd surfaces, *Surf. Sci.* 514 (2002) 409–413.
- [12] T. Matsushima, A. Kokalj, H. Orita, T. Kubo, M. Sakurai, T. Kondo, J. Nakamura, N₂ emission-channel change in NO reduction over stepped Pd(211) by angle-resolved desorption, *Surf. Sci.* 606 (2012) 1029–1036.
- [13] L. Ling, Z. Zhao, X. Feng, Q. Wang, B. Wang, R. Zhang, D. Li, Insight into the reduction of NO by H₂ on the stepped Pd(211) surface, *J. Phys. Chem. C* 121 (2017) 16399–16414.
- [14] X. Liu, D. Tian, S. Ren, C. Meng, Structure sensitivity of NO adsorption–dissociation on Pd_n(n=8, 13, 19, 25) clusters, *J. Phys. Chem. C* 119 (2015) 12941–12948.
- [15] X. Liu, D. Tian, C. Meng, DFT study on the adsorption and dissociation of H₂ on Pd_n (n = 4, 6, 13, 19, 55) clusters, *J. Mol. Struct.* 1080 (2015) 105–110.
- [16] A.M. Doyle, S.K. Shaikhutdinov, S.D. Jackson, H.J. Freund, Hydrogenation on metal surfaces: why are nanoparticles more active than single crystals? *Angew. Chem. Int.*

- Ed. 42 (2003) 5240–5243.
- [17] K.M. Choi, T. Akita, T. Muzagaki, K. Ebitani, K. Kaneda, Highly selective oxidation of allylic alcohols catalyzed by monodispersed 8-shell Pd nanoclusters in the presence of molecular oxygen, *New J. Chem.* 27 (2003) 324–328.
- [18] H. Yin, H. Tang, D. Wang, Y. Gao, Z. Tang, Facile synthesis of surfactant-free Au cluster/graphene hybrids for high-performance oxygen reduction reaction, *ACS Nano* 6 (2012) 8288–8297.
- [19] L. Ouyang, P. Tian, G. Da, X. Xu, C. Ao, T. Chen, R. Si, J. Xu, Y. Han, The origin of active sites for direct synthesis of H₂O₂ on Pd/TiO₂ catalysts: interfaces of Pd and PdO domains, *J. Catal.* 321 (2015) 70–80.
- [20] W. Zhao, F.H. Tian, X. Wang, L. Zhao, Y. Wang, A. Fu, S. Yuan, T. Chu, L. Xia, J.C. Yu, Y. Duan, Removal of nitric oxide by the highly reactive anatase TiO₂(001) surface: a density functional theory study, *J. Colloid Interf. Sci.* 430 (2014) 18–23.
- [21] U.S. Ozkan, M.W. Kumthekar, G. Karakas, Characterization and temperature-programmed studies over Pd/TiO₂ catalysts for NO reduction with methane, *Catal. Today* 40 (1998) 3–14.
- [22] K. Fujiwara, U. Müller, S.E. Pratsinis, Pd subnano-clusters on TiO₂ for solar-light removal of NO, *ACS Catal.* 6 (2016) 1887–1893.
- [23] S. Roy, M.S. Hegde, S. Sharma, N.P. Lalla, A. Marimuthu, G. Madras, Low temperature NO_x and N₂O reaction by H₂: mechanism and development of new nano-catalysts, *Appl. Catal. B-Environ.* 84 (2008) 341–350.
- [24] N. Macleod, R.M. Lambert, Low-temperature NO_x reduction with H₂ + CO under oxygen-rich conditions over a Pd/TiO₂/Al₂O₃ catalyst, *Catal. Commun.* 3 (2002) 61–65.
- [25] N. Macleod, R. Cropley, R.M. Lambert, Efficient reduction of NO_x by H₂ under oxygen-rich conditions over Pd/TiO₂ catalysts: an in situ DRIFTS study, *Catal. Lett.* 86 (2003) 69–75.
- [26] J.Q. Wen, T. Xia, H. Zhou, J.F. Wang, A density functional theory study of small bimetallic Pd_nAl(n = 1–8) clusters, *J. Phys. Chem. Solids* 75 (2014) 528–534.
- [27] G. Qiu, M. Wang, G. Wang, X. Diao, D. Zhao, Z. Du, Y. Li, Structure and electronic properties of Pd_n clusters and their interactions with single S atom studied by density-functional theory, *J. Mol. Struct. Theochem* 861 (2008) 131–136.
- [28] G. Kresse, J. Furthmüller, Efficiency of ab-initio total energy calculations for metals and semiconductors using a plane-wave basis set, *Comp. Mater. Sci.* 6 (1996) 15–50.
- [29] G. Kresse, J. Furthmüller, Efficient iterative schemes for ab initio total-energy calculations using a plane-wave basis set, *Phys. Rev. B* 54 (1996) 11169–11186.
- [30] J.P. Perdew, K. Burke, M. Ernzerhof, Generalized gradient approximation made simple, *Phys. Rev. Lett.* 77 (1996) 3865–3868.
- [31] G. Kresse, D. Joubert, From ultrasoft pseudopotentials to the projector augmented-wave method, *Phys. Rev. B* 59 (1999) 1758–1775.
- [32] P.E. Blöchl, Projector augmented-wave method, *Phys. Rev. B* 50 (1994) 17953–17979.
- [33] S.V. Ong, S.N. Khanna, Origin of oxidation and support-induced structural changes in Pd_n clusters supported on TiO₂, *J. Phys. Chem. C* 115 (2011) 20217–20224.
- [34] R. Zhang, M. Peng, B. Wang, Catalytic selectivity of Rh/TiO₂ catalyst in syngas conversion to ethanol: probing into the mechanism and functions of TiO₂ support and promoter, *Catal. Sci. Technol.* 7 (2017) 1073–1085.
- [35] L. Fernández-Werner, R. Faccio, A. Juan, H. Pardo, B. Montenegro, Á.W. Momburú, Ultrathin (001) and (100) TiO₂(B) sheets: surface reactivity and structural properties, *Appl. Surf. Sci.* 290 (2014) 180–187.
- [36] M.A. Saqlain, A. Hussain, M. Siddiq, A.R. Ferreira, A.A. Leitão, Thermally activated surface oxygen defects at the perimeter of Au/TiO₂: a DFT+U study, *Phys. Chem. Chem. Phys.* 17 (2015) 25403–25410.
- [37] W. Chen, P. Yuan, S. Zhang, Q. Sun, E. Lian, Y. Jia, Electronic properties of anatase TiO₂, doped by lanthanides: a DFT+U study, *Physica B* 407 (2012) 1038–1043.
- [38] J. Yang, C.Q. Lv, Y. Guo, G.C. Wang, A DFT+U study of acetylene selective hydrogenation on oxygen defective anatase(101) and rutile(110) TiO₂ supported Pd₄ cluster, *J. Chem. Phys.* 136 (2012) 104107.
- [39] M.M. Islam, M. Calatayud, G. Pacchioni, Hydrogen adsorption and diffusion on the anatase TiO₂(101) surface: a first-principles investigation, *J. Phys. Chem. C* 115 (2011) 6809–6814.
- [40] K.C. Galbreath, C.J. Zygarlicke, Mercury transformations in coal combustion flue gas, *Fuel Process. Technol.* 65–66 (2000) 289–310.
- [41] E.J. Granite, H.W. Pennline, R.A. Hargis, Novel sorbents for mercury removal from flue gas, *Ind. Eng. Chem. Res.* 39 (2000) 1020–1029.
- [42] R. Zhang, Z. Liu, L. Ling, B. Wang, The effect of anatase TiO₂ surface structure on the behavior of ethanol adsorption and its initial dissociation step: a DFT study, *Appl. Surf. Sci.* 353 (2015) 150–157.
- [43] Z. Zheng, H. Liu, J. Ye, J. Zhao, E.R. Waclawika, H. Zhu, Structure and contribution to photocatalytic activity of the interfaces in nanofibers with mixed anatase and TiO₂(B) phases, *J. Mol. Catal. A-Chem.* 316 (2010) 75–82.
- [44] Y. Ortega, D.F. Hevia, J. Oviedo, M.A. San-Miguel, A DFT study of the stoichiometric and reduced anatase(001) surfaces, *Appl. Surf. Sci.* 294 (2014) 42–48.
- [45] L. Huai, C. He, H. Wang, H. Wen, W. Yi, J. Liu, NO dissociation and reduction by H₂ on Pd(111): a first-principles study, *J. Catal.* 322 (2015) 73–83.
- [46] Q. Luo, T. Wang, M. Beller, H. Jiao, Hydrogen generation from formic acid decomposition on Ni(211), Pd(211) and Pt(211), *J. Mol. Catal. A-Chem.* 379 (2013) 169–177.
- [47] C.A. Farberow, J.A. Dumesic, M. Mavrikakis, Density functional theory calculations and analysis of reaction pathways for reduction of nitric oxide by hydrogen on Pt(111), *ACS Catal.* 4 (2014) 3307–3319.
- [48] D.D. Hibbitts, R. Jiménez, M. Yoshimura, B. Weiss, E. Iglesia, Catalytic NO activation and NO-H₂ reaction pathways, *J. Catal.* 319 (2014) 95–109.
- [49] N.R. Avery, An EELS study of N₂O adsorption on Pt(111), *Surf. Sci.* 131 (1983) 501–510.
- [50] P. Väterlein, T. Krause, M. Bäßler, R. Fink, E. Umbach, J. Taboriski, V. Wüstenhagen, W. Wurth, Adsorption-induced bending of a triatomic molecule: near-edge X-Ray absorption fine structure spectroscopy investigation of N₂O adsorbed on different Ni(111) surfaces, *Phys. Rev. Lett.* 76 (1996) 4749–4752.